

Dual-Input Isolated Full-Bridge Boost DC-DC Converter based on the Distributed Transformers

A. Richard Pravin
Assistant Professor

P. Muthu Kumar
UG Student
Department of Electrical and Electronics Engineering
st. Anne's College of Engineering and Technology
Panruti, Tamil nadu, India.

E. Karthick
UG Student

Abstract: In this paper, a new two-input isolated boost dc-dc converter based on a distributed multi-transformer structure which is suitable for hybrid renewable energy systems is investigated and designed. With a novel transformer winding-connecting strategy, the two input ports can be decoupled completely, so the proposed converter can draw the power from the two different dc sources, which have low output voltage, and transfer it to the dc bus, which has high voltage, separately or simultaneously. The detailed operation principles of the proposed converter have been analyzed in the dual-input mode and the single-input mode, respectively. The main advantage of the proposed topology is that the four transformers and the secondary rectifiers are fully utilized whether the converter is connected with two input power sources or only one input. Although the four transformers are employed, the nominal powers of each transformer and rectifier are both reduced by four times. Furthermore, some special issues on converter design, such as increasing number of the input ports, the magnetic integration and the ground loop decoupling are discussed.

Key words:- Current-fed, DC-DC converter, isolated, multiple inputs, transformer.

1. INTRODUCTION

Nowadays, clean and renewable energies including fuel cell, wind energy, photovoltaic, etc., have been widely applied to achieve environment friendly objectives [1] [2]. Because of the discontinuity of renewable sources, like wind energy and solar energy, generally, an auxiliary power supply is necessary to 1 smooth output power and keep output voltage stable under various load conditions. Thus, an efficient combination of different energy sources, to be a hybrid renewable

power conversion system, has become an interesting topic [3]. Moreover, high power solar cells or fuel cells are often faced with a need of boosting their low output voltage to a high dc-link voltage subjected to the requirements in grid-connecting applications [4].

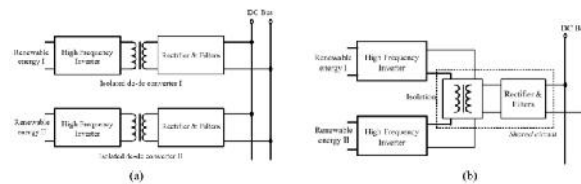


Fig. 1: Block diagram of the systems with two input power sources: (a) Structure based on two isolated individual converters, (b) structure based on the isolated multiple-port structure.

In the last decade, various hybrid system structures have been proposed. For the applications with galvanic isolations, basically, high frequency isolated converters with different input sources can be connected in parallel on a mutual dc bus and thereby each sub-converter can be designed as an individual power module. The block diagram of this system is shown in Fig. 1 (a). The main disadvantage of this system is that if one input source is connected, only one converter will be operated and the other one will be completely under the idle condition that will reduce the power density of the whole system. Due to this reason, multi-port converters have been proposed and received more and more attention in recent years. In these topologies, some parts of the dc-dc converters (such as rectifiers and filters) can be utilised by different input ports mutually, as shown in Fig. 1 (b). Although it will cause complex system control, the power density of the system can be increased in some applications. For the sustainable energy with a low output terminal voltage such as fuel cell, a boost-type converter is favorable for a high efficiency operation. A multi-input isolated boost dc-dc converter with multi-windings based on

the flux additive concept was proposed in [5], but the reverse current block diode is connected in series with the MOSFETs on the primary side, which makes the bidirectional power flow impossible, so the auxiliary circuit for rechargeable elements is needed. In [6], a high step-up isolated converter with two input sources was investigated, and the converter utilizes the current-source type applying to both of the input power sources. To avoid the switch voltage spikes caused by the leakage inductor, an active clamping circuit is added.

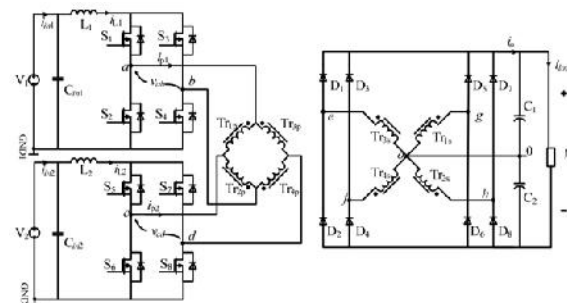
The aim of this paper is to investigate an innovative dual-input full-bridge isolated dc-dc converter [7] for a hybrid renewable energy system. With the novel winding connection and the interleaved PWM modulation strategy, two current-fed power sources with low input voltage can deliver the power to the high voltage dc bus or the load, individually or simultaneously. In this paper, firstly, a review on the state of the art of the multiple-input isolated converters is given to express the background and novelty of this research work. Then, based on the proposed topology, a detailed analysis of the steady-state operation principles of the converter is given and hereby the characteristics of the converter are explained in depth. In order to improve the converter performance further, some issues such as the input port extension, the magnetic integration and the common mode current deduction, which affect the hardware design in practice, are discussed, and some possible solutions are presented. The operating performance of the proposed dual-input converter is examined and is validated through some computer simulations. Using the above study procedure, the salient features of the proposed converter can be summarized: a high step-up ratio, an electric isolation between the clean energy and output voltage, multiple input power sources, and magnetic integration.

2. BASIC PRINCIPLE AND STEADY-STATE OPERATION

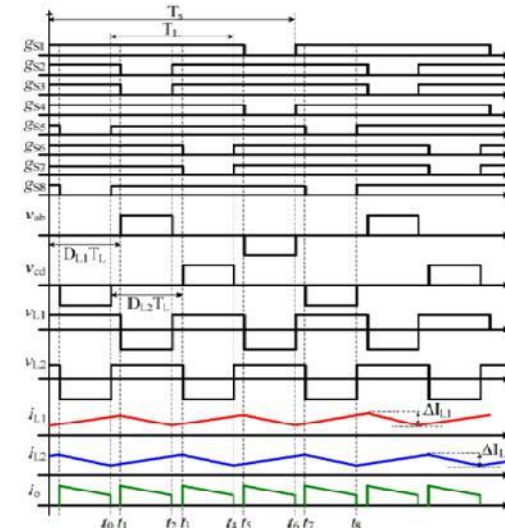
As shown in Fig. 2 (a), the proposed dc-dc converter consists of two boost inductors, two high frequency full-bridge inverters, four transformers and a common output-stage circuit. It is driven by two dc voltage sources, that when associated with large inductors become dc current sources. $Tr1 \# Tr4$ are four identical transformers with same number of turns and turns ratio. According to the converter's operation, its operating principles can be analysed with two different modes: dual-input mode and single input mode.

2.1 Dual-Input Mode

The timing diagrams and the basic operating waveforms in this mode are shown in Fig. 2 (b). There is 180° phase shift between each pair of drive signals, namely $S1, S4$ and $S2, S3$. The switches $S5$ to $S8$ have the same operating principle with that of $S1$ to $S4$. It is worth noting that when the switches in the diagonal position in one of the H-bridges form a simultaneous conduction switch pair to transfer power to the secondary side, it will cause every transformer winding current on the primary side to be clamped as $I1$ or $I2$. The appearance of the clamped current will disable the normal operation of the other dc input-stage circuit, because the current sources can not be connected in series, which means two input ports can not transfer power at same time. To solve this problem, the phase-shift PWM scheme is utilized, which gives 90° phase shift between $S1$ and $S5$. With that, the two input power sources can deliver power to the secondary side simultaneously.



(a) The proposed converter topology



(b) Timing diagrams of the basic operating waveforms in steady state

Fig. 2: Topology and operation of the proposed dual-input isolated boost converter.

In subinterval (t_0-t_1) , all the eight primary side switches operate in their ON states. As shown in Fig. 3 (a), the inductors L_1 and L_2 connect across the dc input sources V_1 and V_2 , respectively. With primary and secondary coils shorted, all the diodes on the secondary side are reverse-biased. Here, two input inductors are charged by the input sources and no power is delivered to the secondary side. Thus, the load current is provided by the output capacitors C_1 and C_2 . The primary inductor currents $iL_1(t)$ and $iL_2(t)$ can be expressed respectively as

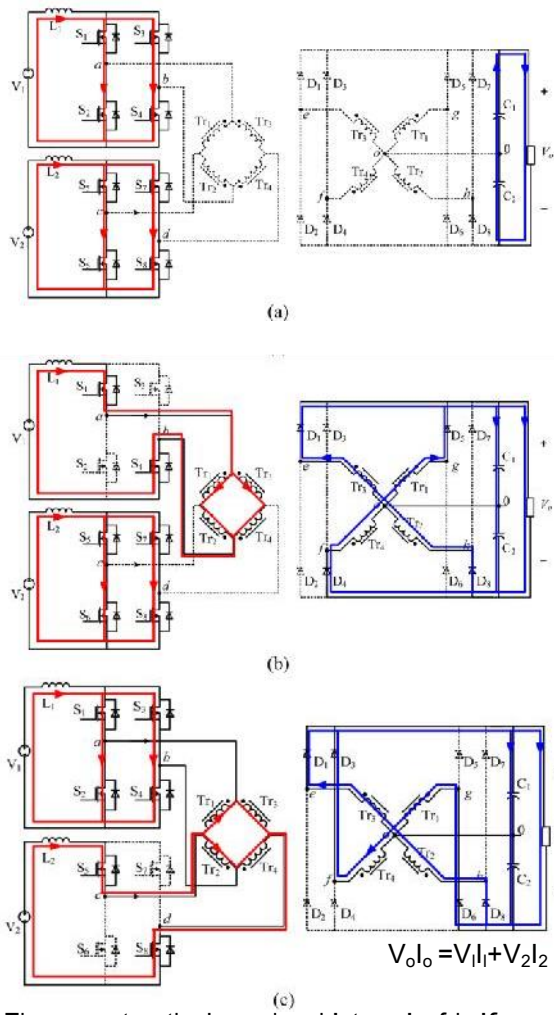


Fig. 3: The current paths in each subinterval of half period: (a) (t_0-t_1) ; (b) (t_1-t_2) ; (c) (t_3-t_4) .

$$i_{L1} \ t = I_{L1} + 0.5\Delta i_{L1} + \frac{V_1}{L_1}(t - t_1) \quad (1)$$

$$i_{L2} \ t = I_{L2} + 0.5\Delta i_{L2} + \frac{V_2}{L_2}(t - t_0) \quad (2)$$

During the second subinterval (t_1-t_2) , S_2 and S_3 operate in their OFF states so that the inductor L_1 is connected via the transistors Tr_1 and Tr_2 through the paralleled paths: one is Tr_1 in series with Tr_2 and the other one is Tr_3 in series with Tr_4 . On the secondary

side, the diodes D_1 , D_4 , D_5 , and D_8 are forward-biased to carry the output current. Thus, v_{ab} is clamped to V_{0n} , and v_{cd} is clamped to 0, where n is the turn ratio of transformer. The current paths are plotted in Fig. 3 (b). $iL_2(t)$ can be expressed as same as that in subinterval (t_0-t_1) , and $iL_1(t)$ is calculated by

$$i_{L1} \ t = I_{L1} + 0.5\Delta i_{L1} + \frac{(V_1 - \frac{V_0}{n})}{L_1}(t - t_1) \quad (3)$$

In subinterval (t_2-t_3) , all the switches on the primary side are turned on, so the operation principle is same to that in (t_0-t_1) and the equivalent current paths can also be illustrated by Fig. 3(a).

During the subinterval (t_3-t_4) , S_6 and S_7 operate in their OFF states so that the inductor L_2 is connected via the transistors S_5 and S_8 through the paralleled paths: one is Tr_2 in series with Tr_4 and the other one is Tr_1 in series with Tr_3 . On the secondary side, the current flows through the diodes D_1 , D_3 , D_4 and D_8 to the dc output, as shown in Fig. 3 (c). So v_{cd} is clamped to V_{0n} and v_{ab} is clamped to 0. $iL_1(t)$ and $iL_2(t)$ are given,

$$i_{L1} \ t = I_{L1} + 0.5\Delta i_{L2} + \frac{V_1}{L_1}(t - t_2) \quad (4)$$

$$i_{L2} \ t = I_{L2} + 0.5\Delta i_{L2} + \frac{(V_2 - \frac{V_0}{n})}{L_2}(t - t_3) \quad (5)$$

Having described the subintervals in a half period, the operating principle of each subinterval in the second half period is similar.

The proposed converter can be completely decoupled into two independent isolated boost converters based on the utilized winding connection and the interleaved PWM modulation strategy. Neglecting all the losses, the output power P_0 is the summation of the input power P_1 and P_2 and can be expressed as

$$(6) P_0 = P_1 + P_2$$

The derived large-signal, small-signal and steady-state models of the proposed converter as well as the detailed design procedure of the voltage and current closed-loop controllers can be found in [8].

2.2 Single-Input Mode

The single-input mode can be seen as a special condition of the double-input mode and its equivalent circuit is shown in Fig. 4. The operation principle in single-input mode is similar to that of the conventional isolated boost converter with H-

bridge input circuit [9]. In order to ensure the ON states of the switches overlap, the switch duty cycle D_s has to be bigger than 0.5. Hence there is a continuous current path for the inductor $L1$. The conversion ratio of the converter in the continuous current mode (CCM) is

$$\frac{V_0}{V_1} = \frac{n}{1-D_L} = \frac{n}{2} \frac{1}{1-D_s} \quad (7)$$

As we can see, all the four transformers can also be utilized completely in the single-input mode. Hereby, the proposed converter has the potential ability to achieve high power density, in comparison to the system consisting of two individual isolated boost converters in parallel. This is true especially for high power applications, where the main power stage is fully used both in dual-input and single-input conditions.

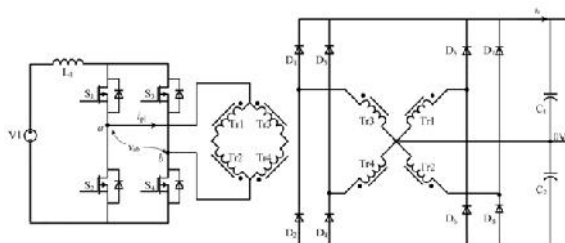


Fig. 4: The equivalent circuit in single-input mode of the converter.

3. SPECIAL ISSUES ON THE CONVERTER DESIGN

To improve the performance of the proposed dc-dc converter, some practical issues such as how to reduce the inductive elements, extending the number of inputs and common mode current deduction are discussed below.

3.1 Magnetic Integration

The complex winding connection makes an optimal layout of the primary side difficult. But by an effective magnetic integration, the number of the inductive elements can be reduced [10]. In the dual-input mode, the voltages across every primary winding are listed in Table 1.

Table 1 Voltages across each primary winding

Subintervals	V_{Tr1a}	V_{Tr2a}	V_{Tr3a}	V_{Tr4a}
(t_1-t_2)	$+V_0/2n$	$-V_0/2n$	$+V_0/2n$	$-V_0/2n$
(t_3-t_4)	$-V_0/2n$	$-V_0/2n$	$+V_0/2n$	$+V_0/2n$
(t_5-t_6)	$-V_0/2n$	$+V_0/2n$	$-V_0/2n$	$+V_0/2n$
(t_7-t_8)	$+V_0/2n$	$+V_0/2n$	$-V_0/2n$	$-V_0/2n$

It can be seen that windings $Tr1a$ and $Tr4a$ as well as $Tr2a$ and $Tr3a$ always have opposite voltage. In order to reduce the transformer footprint area and increase the power density, the two input inductors $L1$ and $L2$, and the four individual transformers, $Tr1$, $Tr4$, and $Tr2$, $Tr3$, can be wound with two sets of E-I- E cores, shown in Fig. 5 (a). The windings of each transformer are equally divided into the outer legs of E-cores. In transformer $Tr1$, $P1/2$ and $S1/2$ represent the half of primary winding and the half of secondary winding respectively. $P4/2$ and $S4/2$ are the same properties for the transformer $Tr4$. $L1-1$ in parallel with $L1-2$ wound in the center legs of E-cores to form the boost inductor $L1$. The middle I-core provides a shared flux return path. @1 and @4 represent ac flux generated by the transformers $Tr1$ and $Tr4$ respectively.

By arranging the directions of the windings on the outer legs for each transformer, zero ac flux can be achieved in the centre legs. @1 and @4 have their own flux paths due to a low reluctance path provided by shared I-core meaning the two transformers $Tr1$ and $Tr4$ are uncoupled. Because @1 is equivalent to @4 in this work, the ac flux will partially cancel in shared I-core. The dc flux @ $L1$ generated by the inductor $L1$ goes

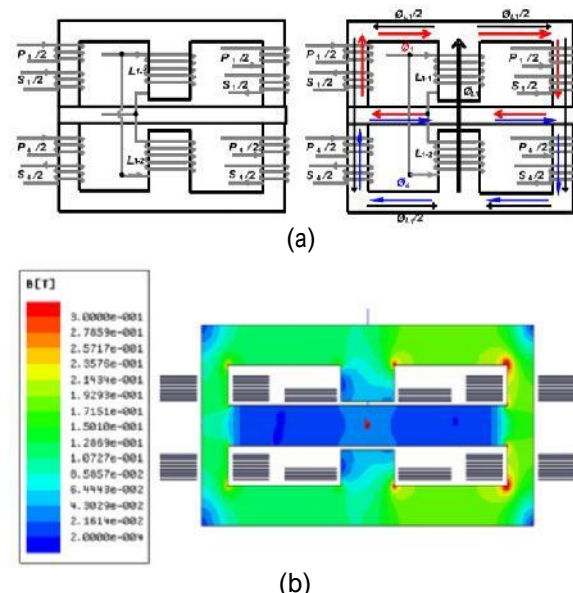


Fig. 5: Two transformers and one input inductor in E-I-E integration, (a) winding arrangement; (b) 2D simulation by FEA analysis.

through the centre legs of E cores. Half of @ $L1$ runs in the outer legs of the E-cores and no dc flux exists in the shared I-core due to complete cancellation effect. To verify the validity of the proposed design approach and theoretical analysis, a 2D simulation

model linked with external circuit has been built in a finite element analysis (FEA) tool. As shown in Fig. 5 (b), the right side has higher flux density B because half of $@L1$ adds to $@1$ and $@4$ but on the left side, these fluxes subtract. In the shared I core, $@1$ and $@4$ cancels out. Hence, based on this magnetic integration idea, the four transformers and two inductors can be integrated into two sets of E-I-E cores. It reduces the number of magnetic elements as well as the core losses. More detailed design procedure can be found in [10].

3.2 Method to Increase the Number of Inputs

The primary and secondary windings of the transformers from the Fig. 2 are re-illustrated in Fig.

6(a). The voltage vector across the different terminals, from a to d on primary side, and the current vectors, from e to h on secondary side can be plotted in Fig. 6 (b), where the employed primary windings are numbered as 1-4. According to the operating sequence, the potential and current vectors will rotate clockwise like a 2-pair-pole dc motor. Based on this simplified model, the other 2-pair poles can be added symmetrically in the system with a phase shift: 45 degree electrical angle, as shown in Fig. 6 (c), and thereby the proposed dual-input converter can be extended to a converter with 4 input ports by the winding connection shown in Fig. 6 (d). Thus, the number of inputs N_{input} and the corresponding number of transformer N_{Tr} can be derived as

$$N_{\text{input}} = 2^m \quad (m=1,2,\dots)$$

$$N_{\text{Tr}} = 2 N_{\text{input}} \quad (8)$$

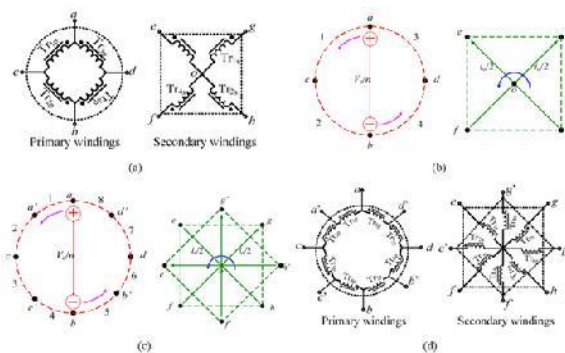


Fig. 6: Method to increase the number of inputs: (a) windings for two inputs, (b) equivalent voltage and current vectors for two inputs, (c) equivalent voltage and current vectors for four inputs, (d) windings for four inputs.

It is worth noting that: 1) the number of inputs must be exponent of 2; 2) with increasing number of input ports, the number of the transformers is increased by twice that of input ports. If the converter has multiple inputs, utilizing the high order magnetic integration method can simplify the converter circuit further, but it is out of scope of this paper and will not be discussed here.

4 Observations and simulation Results

Fig. 7 shows Simulink/PLECS simulation results. Simulation parameters are based on the above design parameters ($V1=V2=30V$ and $V0=400V$). The simulation results in Fig. 7 agree with the theoretical analysis described in section 2.

The experimental waveforms are shown in Fig. 12. In the single input mode with 50 V input voltage, Fig. 8(a) shows the primary side voltage and current, i.e. v_{ab} and i_{p1} , which have been annotated in Fig. 2. While Fig. 8(b) shows the plots of the primary voltages v_{ab} and v_{cd} , and primary current i_{p1} and i_{p2} in the dual-input mode with the conditions: $V1=50V$ and $V2=30V$, which verifies the theoretical analysis results that two input voltage sources can deliver the power together.

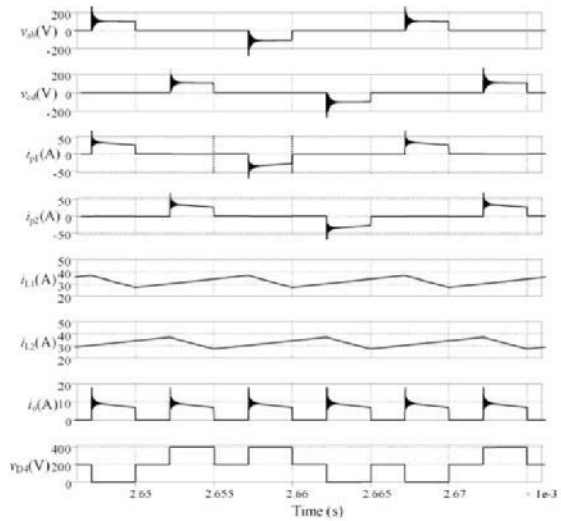
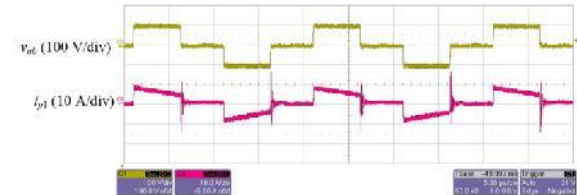


Fig. 7: Simulation results – v_{ab} , v_{cd} , i_{p1} , i_{p2} , i_{L1} , i_{L2} , i_D and v_{D4} .



(a)Primary side voltage and current under single – input mode(time base: 5 us/div)

The efficiencies are measured without including the gate driver losses, and presented in Fig. 13. The efficiency curves with respective to the input voltage in the single input mode are plotted in Fig. 9(a). It exhibits a maximum efficiency of 96.5% with 50 V input, and the measured efficiency is 92.1% at 1500 W with 30 V input.

The measured efficiency curve of the converter with the conditions: input voltages $V1=V2=30$ V, output voltage of 400 V, and $P1 \approx P2$, are shown in Fig. 13 (b). Comparing to the efficiency curves shown in Fig. 13(a), in dual-input mode, the measured efficiency is about 92.4% at the output power of 200 W, which is lower than that in single-input boost mode because of higher switching losses. But at high output power, the efficiency is higher in dual-input operation mode, which is around 94.0% ($Po=1450$ W). Fig. 13 (c) shows the measured efficiency with input voltages $V1=50$ V, $V2=30$ V, output voltage of 400 V, and input power $P1 \neq P2$. The maximum efficiency is measured as 95.7%.

5. CONCLUSION

There are some solutions to the multi-input-port voltage-fed or current-fed isolated converters which can be utilized in the applications in which hybrid sustainable energy sources involved. Comparing to the existing topologies, the converter proposed in this paper has the promising points: the lower input current ripple, two controllable independent input power ports (can be extended to multiple ports), the symmetrical circuit structure which is favourable to achieving magnetic integration and modularizing. The most prominent characteristic of the proposed converter is that the main power flow path, consisting of 4 transformers and full bridge rectifier, is shared by both of the input ports, and the nominal power of each transformer and rectifier can be reduced, so a higher power density can be achieved. There are still some negative sides such as complex transformer windings connection and no common ground, and in the future research, the dc offset of transformers caused by unbalance on the voltages or the switching times has to be investigated in depth. Overall, the proposed converter is one of the promising candidate circuits, and is suitable to the applications with hybrid renewable energies.

REFERENCES

- [1] [1]F. Blaabjerg, Z. Chen, and s. B. Kjaer, "Power electronics as efficient interface in dispersed power generation systems," *IEEE Trans. Power Electron.*, 2004, 19, (5), pp. 1184-1194.
- [2] Z. Chen, J. Guerrero, and F. Blaabjerg, "A review of the state of the art of power electronics for wind turbines," *IEEE Trans. Power Electron.*, 2009, 24, (8), pp. 1859-1875.
- [3] M. Bragard, N. Soltau, S. Thomas and R. W. De Doncker, "The balance of renewable sources and user demands in grids: power electronics for modular battery energy storage systems," *IEEE Trans. Power Electron.*, 2010, 25, (12), pp. 3049- 3056.
- [4] H. Cha, J. Choi and P. N. Enjeti, "A three- phase current-fed DC/DC converter with active clamp for low-dc renewable energy sources," *IEEE Trans. Power Electron.*, 2008, 23, (6), pp.2784-2793.
- [5] Z. Qian, O. Abdel-Rahman, H. Al-Atrash, and I. Batarseh, "Modeling and control of three- port DC/DC converter Interface for satellite applications," *IEEE Trans. Power Electron.*, 2010, 25, (3), pp.637-649.
- [6] Y.C.Liu and Y.M. Chen, "A systematic approach to synthesizing multi-input DC-DC converters," *IEEE Trans. Power Electron.*, 2009, 24, (1), pp. 116-127.
- [7] Y. Li, X. Ruan, D. Yang, F. Liu and C. K. Tse, "synthesis of multiple-input DC/DC converters," *IEEE Trans. Power Electron.*, 2010, 25, (9), pp. 2372-2385.
- [8] H. Tao, J. L. Duarte and M. A. M. Hendrix, "Three-port triple-half-bridge bidirectional converter with zero-voltage switching," *IEEE*
- [9] M. Nyman, R. Tranberg, M. E. Madsen, U. K. Madawala, M. A. E. Andersen, "What is the best converter for low voltage fuel cell applications- A buck or boost," *Proc. Annual Conference of the IEEE Industrial Electronics Society*, 2009, pp. 959-964.
- [10] Z.Zhang, O. C. Thomsen and M. A. E. Andersen, "Modeling and control of a dual-Input isolated full-bridge boost converter," *Proc. Applied Power Electronics Conf. and Exposition*, 2012. (in press)
- [11] V.Vaisanen, T.Riipinen and P. Silventoinen, "Effects of switching asymmetry on an isolated full-bridge boost converter," *IEEE Trans. Power Electron.*, 2010, 25, (8), pp. 2033-2044. Z. Ouyang, Z. Zhang, O. C. Thomsen, M. A. E. Andersen, "Planar integrated magnetics (PIM) module in hybrid bidirectional DC/DC converter for fuel cell application," *IEEE Trans. On Power Electron.*, 2011, 26, (11), pp.3254-3264.